

Localization through Surface Folding in Solid Foams under Compression

P. M. Reis,^{1,*} F. Corson,² A. Boudaoud,² and B. Roman³

¹*Department of Mathematics, Massachusetts Institute of Technology, Cambridge, Massachusetts 02139, USA*

²*Laboratoire de Physique Statistique, École Normale Supérieure, UPMC Paris 06, Université Paris Diderot, CNRS, 24 rue Lhomond, 75005 Paris, France*

³*PMMH, CNRS UMR 7636, ESPCI, ParisTech, Univ. Paris 6 & Paris 7, 10 Rue Vauquelin, 75231 Paris Cedex 05, France*

(Received 11 March 2009; published 22 July 2009)

We report a combined experimental and theoretical study of the compression of a solid foam coated with a thin elastic film. Past a critical compression threshold, a pattern of localized folds emerges with a characteristic size that is imposed by an instability of the thin surface film. We perform optical surface measurements of the statistical properties of these localization zones and find that they are characterized by robust exponential tails in the strain distributions. Following a hybrid continuum and statistical approach, we develop a theory that accurately describes the nucleation and length scale of these structures and predicts the characteristic strains associated with the localized regions.

DOI: 10.1103/PhysRevLett.103.045501

PACS numbers: 62.20.D-, 46.70.De, 61.43.Gt, 62.20.mq

In many symmetry-breaking systems [1], a large scale homogeneous energy input or loading may result in spontaneous localization, into small regions. Examples include the crumpling of thin sheets [2], fracture through drying [3], or uniaxial loading and dielectric breakdown [4]. Often, these localized zones can appear with no characteristic length scale, and may then progressively invade the system for increasing loads (e.g., localization in cellular solids [5], force chains in granular materials [6], and thermodynamic phase transitions) or remain single absorbing structures (uniaxial fracture, dielectric breakdown, floating folds [7]). However, in another general class of localization phenomenon, structures form with a characteristic size, and their number then increases with loading (e.g. crumpling singularities, drying cracks). These instances of pattern-forming localization are involved in a wide range of applications in biology and technology. Some flexible electronic applications [8], for example, take advantage of localized blistering of thin films deposited on an elastic substrate [9]. Moreover, a related creasing instability has been reported in surface-attached hydrogels [10]. Also, it has recently been suggested that venation networks in leaves reflect patterns of localization under compression [11,12]. A common approach towards understanding this wide range of systems is to identify (i) the mechanism underlying the localization process, (ii) the origin of the length scales involved and (iii) the statistical properties of such structures.

In this spirit, here we consider a novel system where we compress a cellular solid (foam) coated with a thin elastic film. We show that the scaleless classical localization of solid foams under compression can this way be converted into a pattern-forming process with a characteristic length scale. If the substrate were linearly elastic, compressing the sheet would produce sinusoidal buckling and no localization would occur [13]. For a liquid substrate, a single localized fold could appear [7]. In contrast, our solid

foam substrates provide both a nonlinear mechanical response and a natural distribution of heterogeneities [5] where localization is observed. By analogy with localized extensional deformation in fracture, we refer to the localized zones that we observe as anticracks. We study the properties of these anticracks by a combination of well-controlled experiments and a hybrid continuum and statistical description.

In our experiments, we uniaxially compress a block of solid foam with dimensions $120 \times 100 \times 60 \text{ mm}^3$. Since the loading in our study is always compressive (negative strain), for convenience we introduce the notation $\eta = -\epsilon$ for compressive strains. The closed cell polyester foams that we use have individual cell sizes of $\sim 200 \mu\text{m}$ [Fig. 1(c)] and follow a typical mechanical behavior [5] of cellular solids: first a linear stress-strain relation (Young's modulus of $E_b = 6.8 \pm 0.5 \text{ MPa}$), followed by a stress plateau for $\eta > \eta_b$ corresponding to the buckling and crushing of the walls of the unit cells of the foam, the onset of which defines the threshold $\eta_b = (3.95 \pm 0.05) \times 10^{-2}$. At even higher strains, the load increases again, corresponding to the elasticity of the bulk material (polyester) since most of the cells have by now been crushed. An important feature of our experiments is that the front and back faces ($120 \times 100 \text{ mm}^2$) of the foam block are coated with a thin film also of polyester that is chemically bound to the bulk. This film has thickness $h = 310 \pm 20 \mu\text{m}$ and Young's modulus $E_f = 154 \pm 24 \text{ MPa}$. We use an Instron machine to perform uniaxial compression at imposed displacements. Compression is performed at constant Lagrangian strain rate $\dot{\eta}_t = 8.33 \times 10^{-4} \text{ s}^{-1}$, and we measure the total resulting load of the samples.

In Fig. 1(b) we present the nominal stress-strain response curve of our samples (foams with thin crust) under compression. At low strains, the linear elasticity of the sample is probed. Beyond a critical value of the total strain, $\eta_c = (3.45 \pm 0.05) \times 10^{-2}$, a plateau is reached where the

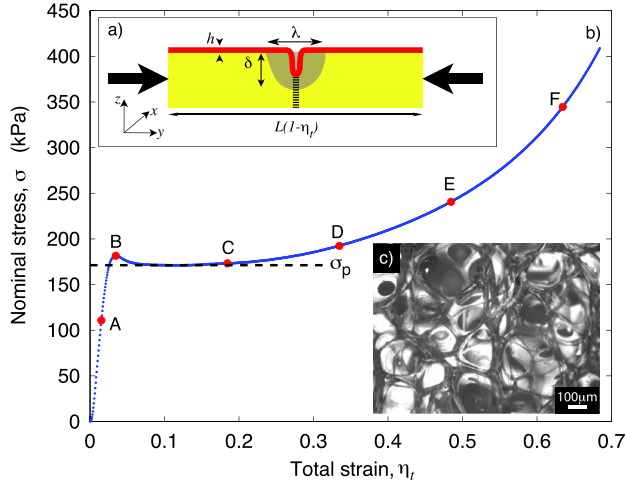


FIG. 1 (color online). (a) Schematic of the experimental setup. The foam block is compressed along the y direction (initial length L). The surface film has thickness h . The folds have width λ and depth δ ; they induce localization in the bulk (dashed vertical line). (b) Stress-strain curve. The plateau stress σ_p is indicated by the dashed line. The points labeled A,B,...,F correspond to the labels in Fig. 2. (c) Micrograph of the polyester foam in the bulk.

load remains approximately constant, $\sigma_p \approx 171$ kPa, with increasing η . Even though the mechanical response of the bulk foam is similar to that with the thin surface film, the onset of localization in the latter occurs slightly earlier; $\eta_c < \eta_b$. Moreover, in the plateau we observe the formation of localization regions at the surface of the sample as sharp folds form. A schematic diagram of such a fold is given in Fig. 1(a). To monitor the local displacement of this surface film, a high-resolution camera (10 MPixels) was synchronized with the Instron to take pictures at 1/6 frames per second. A random array of dots, with sizes ranging from of order 10^{-5} to 10^{-2} m, was spray painted on the surface of the foam blocks. This allowed for in-plane displacements to be measured using a precision image correlation algorithm based on particle image velocimetry (PIV—StrainMaster-Davis, LaVision), a technique commonly used in fluids mechanics.

Figure 2 illustrates the evolution of the surface deformation as the total strain is increased. The pairs of images

(A1, A2) through (F1, F2) are taken at the same values of total strain as the points (A-F) along the stress-strain curve in Fig. 1(b). Images (A1 through F1) show the field of strain increments in the y direction, $\eta_{yy}^E(x, y)$, between successive frames, in the Eulerian (laboratory) frame of reference. The sequence of images (A2, B2, through F2) present the corresponding cumulative strain, $\eta_{yy}^L(x, y)$, in the Lagrangian frame of reference. In Fig. 2 (A1) and (A2), the strain field is homogeneous, corresponding to the initial linear-elastic regime discussed above. Above η_c , regions of strong localization, or anticracks, develop and propagate perpendicular to the direction of compression [14]. In the experiments, the point of onset of surface localization [Fig. 2 (B1) and (B2)] is observed in the vicinity of onset of the plateau in the stress-strain curve (point B in Fig. 1) and $\eta_b \approx \eta_c$. Eventually, the surface of the sample is covered with approximately equally spaced folds. The corresponding characteristic length scale, determined from the FFT of the Lagrangian strain fields along the y direction, is $\lambda_l = 6.5 \pm 0.5$ mm [e.g., in Fig. 2 (F2)].

We now rationalize these observations through scaling analysis. If the (bulk) substrate were linearly elastic, then the film would buckle into a sinusoidal shape (see, e.g., [13]) above a threshold in strain, $\eta_s \sim C^{-2/3}$, where $C = E_f/E_b$ is the ratio of moduli for the film and bulk, respectively. In our case, the solid foam might undergo localization under compression [5]. Thus, we consider the appearance of a single fold of width λ and depth δ , as shown in the schematic diagram of Fig. 1(a). This yields a characteristic strain in the fold along the y direction, $s \sim (\delta/\lambda)^2$, that releases a compressive stress $\sigma_f \sim E_f \eta$ in the film and corresponds to a gain in energy density (per unit surface) of $\sigma_f s \sim E_f \eta \delta^2 / \lambda^2$. The appearance of a localized zone in the foam, costs a displacement δ against the plateau stress $\sigma_p \sim E_b \eta_b$, where η_b is the strain threshold for bulk localization. The resulting energy density is $E_b \eta_b \delta$. As will be clarified below, one may neglect the bending energy of the film. The total elastic energy can now be written as

$$\mathcal{E} \sim -E_f h \eta \delta^2 / \lambda + E_b \eta_b \delta \lambda, \quad (1)$$

after combining the two energy density terms and multiplying them by the width of the fold, λ . For a given width

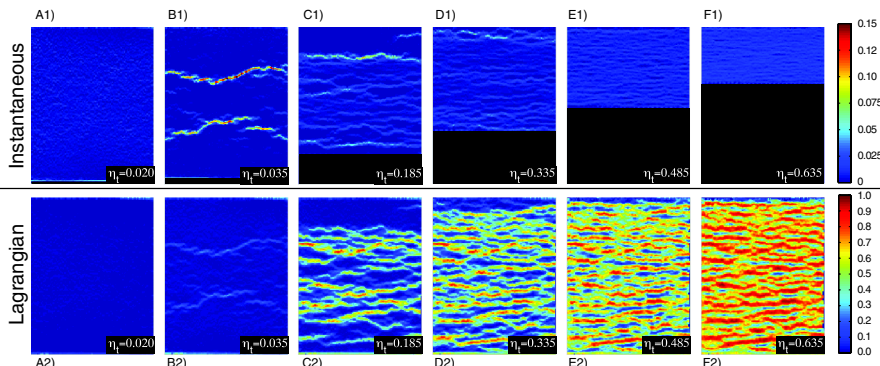


FIG. 2 (color online). (A1) through (F1) Field of strain increments in the y direction between successive frames, $\eta_{yy}^E(x, y)$ (Eulerian frame of reference). (A2) through (F2) corresponding Lagrangian strain field η_{yy}^L , for the same values of compression. The respective value of η is given on the bottom-right corner of each strain field.

λ , this total energy \mathcal{E} increases with δ up to a maximum and then decreases to $-\infty$, so that there is an energy barrier for the nucleation of a fold. This accounts for the observed subcritical nature of the instability, and the fact that localized regions always involve large internal strains.

In the experiments, two mechanisms could help overcome this energy barrier. In the first, sinusoidal buckling would increase the strain beyond η_b in the foam regions close to the troughs. This mechanism is absent here since its threshold, $\eta_s \sim 0.1$, is much larger than the experimental threshold η_c . The second possible mechanism relies on the heterogeneity of the foam and the resulting spatial fluctuations of the bulk localization threshold, η_b . It is more likely that nucleation occurs in a small region close to the crust than across the whole depth of the foam. The threshold for nucleation, η_c , is then given by the smallest value of the fluctuating η_b . This explains that, in our experiments the instability threshold, η_c , occurs in the vicinity of the bulk cellular solid localization threshold, η_b . As a result, once formed, these surface folds act as nucleation sites for localization in the bulk.

When a fold is nucleated, Eq. (1) predicts an infinite depth, δ . However, geometry imposes $\delta < \lambda/2$ since λ is defined in the reference configuration. This implies that, $\delta \sim \lambda$, and the folds are always deep. Consequently, at the instability threshold ($\eta = \eta_c$ and $\delta \sim \lambda$) the total energy takes the form,

$$\mathcal{E} \sim -E_f h \eta_c \lambda + E_b \eta_b \lambda^2, \quad (2)$$

which upon minimization with respect to λ yields,

$$\lambda \sim E_f / E_b \eta_c / \eta_b h \sim Ch \eta_c / \eta_b. \quad (3)$$

This scaling is valid as long as the bending energy, $E_f h^3 / \lambda$, of the film is negligible with respect to other energies, i.e., as long as $C^2 \eta_c^3 \eta_b^{-2}$ is large (here this quantity is of the order of 20). At saturation, all folds are in contact, so that the width λ also sets the typical wavelength of the pattern. Experimentally, we find a saturation wavelength of $\lambda_l = (6.5 \pm 0.5)$ mm, in good agreement with the predicted $Ch \eta_c / \eta_b = (6.1 \pm 1.1)$ mm.

In order to probe the stability of the observed patterns in the experiments, we preindented the film surface with equally spaced and parallel grooves ($\sim 500 \mu\text{m}$ deep). This pattern acted as a template for the nucleation of folds.

As before, we determined the wavelength of the resulting localization patterns, λ_{fit} , from their FFT, at $\eta = 0.38$ compression. In Fig. 3 we show the dependence of this wavelength on the wavelength of the prepattern, λ_p . For large values of λ_p , the pattern selects the same wavelength λ_l that would be obtained without a prepattern. In contrast, for small λ_p , the wavelength of the final pattern coincides with the wavelength of the perturbation. This result still holds for perturbation wavelengths larger than the natural wavelength of the system, breaking down around $\lambda_p = 2\lambda_l$. This indicates that new anticracks can be formed between existing ones by further compression, if and only if they are separated by more than $2\lambda_l$. These obser-

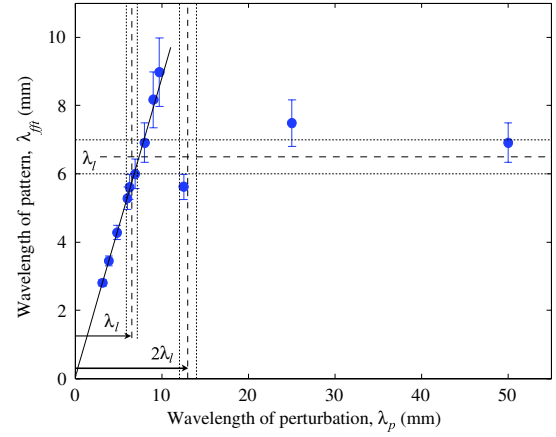


FIG. 3 (color online). Perturbations experiment. Wavelength of the final pattern of anticracks measured from the FFT of the $\eta_{yy}^L(x, y)$ field as a function of the wavelength of the initial perturbation pattern, λ_p . The horizontal and vertical dashed line are located at $\lambda_l = 6.5 \pm 0.5$ mm found for an unperturbed surface, and $2\lambda_l$, respectively (dotted lines correspond to their experimental uncertainty).

vations support the scenario that the folds appear through a nucleation process.

Now we turn to the evolution of the number of folds N with compression. Each new fold accommodates a length $\ell \sim \lambda$ and has a typical strain $s = O(1)$. Consequently, at low strain, the total change in length ηL (L is the sample's total length) is equal to the change of length accommodated by all folds, $N\ell$. Therefore,

$$N = \eta L / \ell, \quad (4)$$

which corresponds to the initial linear evolution in Fig. 4(a) where we plot the average number of folds $N(\eta)$, along y , as a function of total strain. When the folds become in contact, their number cannot increase further and $N(\eta)$ saturates. This happens when the total strain is equal to the strain in the fold. More quantitatively, if we consider folds with a 45° slope, then $\ell = (1 - 1/\sqrt{2})\lambda$ and $s = \ell/\lambda = 0.3$. This yields an initial slope $L/\ell = 59$ [dashed line in Fig. 4(a)] and a saturation at $\eta = 0.3$ [consistent with saturation in Fig. 4(a)] for the evolution of the number of folds $N(\eta)$. Both of these observations are in good agreement with the corresponding experimental values plotted in Fig. 4(a).

Finally, we focus on the statistical properties of these anticracks, as measured by the probability distribution of strain increments. In Fig. 4(b) we plot experimental distribution curves for various values of the total compression. At low compression, in the regime where the strain field is homogeneous, e.g., $\eta = 5 \times 10^{-3}$, this distribution is strongly peaked close to $\eta_{yy}^E = 0$ with a Gaussian-like shape. In contrast, above the localization threshold, the formation and growth of anticracks result in pronounced exponential tails, which can span up to four decades in probability. These distributions can be understood as fol-

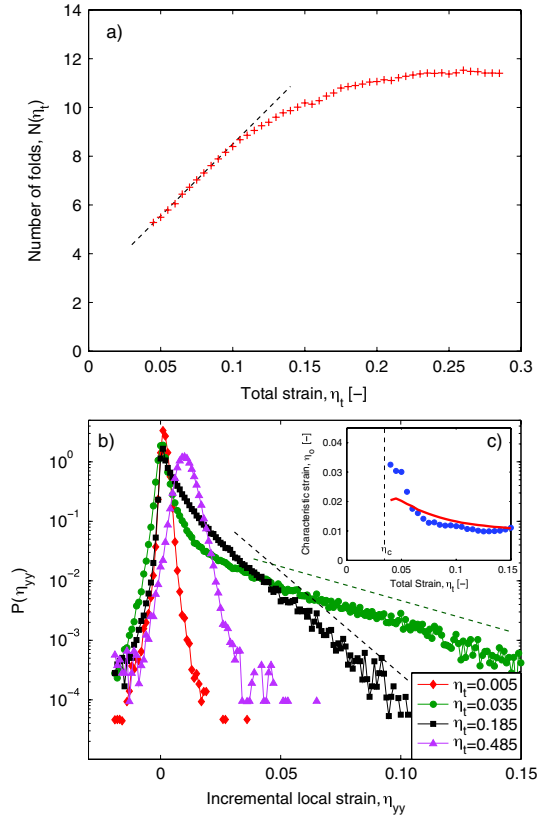


FIG. 4 (color online). (a) Average number of folds N along y as a function of compression. Dashed line has slope $L/\ell = 59$, predicted by Eq. (4). (b) Probability distribution function of strain, η_{yy}^E , at four values of total strain (shown in the legend). (c) Inset: Characteristic strain, η_0 , measured from the inverse of the slope of the exponential tails in (b). Dashed vertical line at threshold, η_c . Solid line predicted by theory in Eq. (5).

lows. Between two consecutive frames, the decrease in length ΔL (where $\Delta = \dot{\eta}\tau$ and $\tau = 6$ s is the time between two frames) is randomly distributed across all N folds, each of them accommodating a random length d . This is analogous to the random distribution of the total energy of a noninteracting classical gas between all particles, hence an exponential distribution for the incremental strain $\eta_{yy}^E = d/\lambda$ [15]. The characteristic strain $\eta_0 = \langle \eta_{yy}^E \rangle$ ($\langle \cdot \rangle$ denotes ensemble averaging) of the exponential can now be predicted by noting that $N\langle d \rangle = \Delta L$ such that,

$$\eta_0 = \frac{\Delta L}{N(\eta)\lambda}. \quad (5)$$

In Fig. 4(c) we summarize the evolution of the characteristic strain associated with the anticracks, η_0 . This was measured from the inverse of the slope of the exponential tails of the distributions. At the localization threshold, the anticracks appear with a large characteristic strain, η_0 , which then gradually decreases as the sample is further compressed. The dependence of η_0 on N_t is compared with the theoretical prediction of Eq. (5), directly using the

measured values of N in Fig. 4(a). The agreement is excellent, except in the vicinity of the threshold, η_c , which is remarkable since there are no fitting parameters. At larger values of compression (e.g., $\eta = 0.485$), as the number of folds saturates and the fields regain homogeneity, the exponential tails disappear and the distribution recovers a Gaussian-like shape.

In conclusion, we have introduced a novel experimental system to study localization in heterogeneous solids. The observed patterns feature a well-defined length scale imposed by an instability of the thin surface film. Moreover, the statistics of the Eulerian strain distributions and, in particular, their pronounced exponential tails are well captured by a hybrid continuum and statistical description. In this system, we were able to identify the localization mechanism and characterize it quantitatively. Having identified and measured the relevant variables, we believe that our study will serve as an important guidance to the understanding of other systems where patterning occurs through mechanical stresses.

This work was funded by the MechPlant NEST-Adventure program of the European Union. We thank M. Adda-Bedia for suggesting the study of localization in foams.

*preis@mit.edu

- [1] J.P. Gollub and J.S. Langer Rev. Mod. Phys. **71**, S396 (1999).
- [2] T. A. Witten, Rev. Mod. Phys. **79**, 643 (2007).
- [3] C. Allain and L. Limat, Phys. Rev. Lett. **74**, 2981 (1995); A. Malthe-Sorensen, T. Walmann, J. Feder, T. Jossang, and P. Meakin, Phys. Rev. E **58**, 5548 (1998).
- [4] M. F. Gyure and P. D. Beale, Phys. Rev. B **46**, 3736 (1992).
- [5] L. J. Gibson and M. F. Ashby, *Cellular Solids: Structure and Properties* (Cambridge University Press, Cambridge, England, 1997).
- [6] J. Geng *et al.*, Phys. Rev. Lett. **87**, 035506 (2001).
- [7] L. Pocivavsek *et al.*, Science **320**, 912 (2008).
- [8] D. H. Kim and J. A. Rogers, Adv. Mater. **20**, 4887 (2008).
- [9] Y. Sun *et al.*, Nature Nanotech. **1**, 201 (2006); D. Vella, J. Bico, A. Boudaoud, B. Roman, and P. M. Reis, Proc. Natl. Acad. Sci. U.S.A. **106**, 10901 (2009).
- [10] V. Trujillo, J. Kim and R. C. Hayward, Soft Matter **4**, 564 (2008).
- [11] M. F. Laguna, S. Bohn, and E. A. Jagla, PLoS Comp. Biol. **4**, e1000055 (2008).
- [12] Y. Couder *et al.*, Eur. Phys. J. B **28**, 135 (2002).
- [13] N. Bowden *et al.*, Nature (London) **393**, 146 (1998).
- [14] Note that a compressed solid foam (with no topping layer) also undergoes localization but that no well-defined length scale appears.
- [15] We have checked that the distributions of the maximum strain increment in each fold are also exponential. This implies that the shape of the distributions is governed by how the imposed displacement is distributed between the folds rather than by the shape of the individual folds.